INSTITUTE OF PHYSICS PUBLISHING JOURNAL OF PHYSICS: CONDENSED MATTER

J. Phys.: Condens. Matter **13** (2001) 7645–7658 PII: S0953-8984(01)27374-3

Lattice dynamics and inelastic nuclear resonant x-ray scattering

E E Alp, W Sturhahn and T S Toellner

Advanced Photon Source, Argonne National Laboratory, Argonne, IL 60439, USA

Received 31 July 2001
Published 9 August 2001
Online at stacks.iop.org/JPhysCM/13/7645

Abstract

Measurements of thermal and elastic properties of materials, such as the phonon density of states, specific heat, and speed of sound, by a new x-ray scattering technique are presented. Inelastic nuclear resonant scattering of x-rays produced from new electron storage rings, coupled with advances in high-energy-resolution crystal optics, and fast detectors have enabled the development of a new method of analysing the energy loss in a scattering process with a resolution of 10^7 or better in the x-ray region of 6–30 keV. Some unique aspects such as element (isotope) selectivity, the amount of material needed for analysis (nanograms), and the physical size to which x-rays can be focused (5 μm or better) favour this approach over the more established techniques of neutron scattering and Mössbauer and Raman spectroscopy. Applications to several unique cases—for example, those of multilayers and high pressure—are discussed.

1. Introduction to thermal and elastic properties of materials

Thermal and elastic properties of materials are directly related to the interaction between ionic cores and the electron gas. Accurate measurement of macroscopic properties such as specific heat, thermal expansion coefficient, and speed of sound is of fundamental importance for understanding the nature of the interaction between nuclei, localized core electrons, and extended valence electrons in solids and liquids. Therefore, any new technique that provides some unique features in measuring thermal and elastic properties provides new opportunities for better understanding and further developing new materials. It is within this context that a relatively new technique based on inelastic nuclear resonant scattering of x-rays will be discussed.

At the time of writing, there are no textbooks that discuss measurement of lattice dynamical properties of materials using this technique. The treatment given here will be concise, mostly referring the reader to papers published in the last decade for details.

The relative oscillations of atoms around their equilibrium position can be described as harmonic oscillations of a hard sphere bound by a given potential. Inherent in this description

are the two main approximations: (a) the *adiabatic approximation* in which the motion of heavier ion cores is treated separately to that of the electrons whose average motion generates the potential that dictates the motion of the ion cores; and (b) the *harmonic approximation* in which only the second-order term in the Taylor expansion of the interatomic potential is retained. This allows description of the motion of ion cores within the formalism of a harmonic oscillator. In the classical mechanical treatment, each normal mode of vibration acts as an independent oscillator. This also applies in the quantum mechanical approach. The quantized energy levels are occupied by excitations called phonons, which are lattice vibrations with frequency ω. The term 'phonon' refers to the relative motion of atoms and not to a net motion of the centre of mass (i.e. diffusion), and phonons do not carry a net momentum as photons do. Phonons, therefore, are called quasi-particles. Since no spin is associated with phonons, they are indistinguishable particles, and obey Bose–Einstein statistics with an occupation number

$$\overline{n_q} = \frac{1}{e^{\hbar\omega(q)/kT} - 1}. \tag{1.1}$$

If there are N atoms, the motion of each atom can be expressed in terms of two transverse and one longitudinal motion, which make up the $3N$ normal modes of vibration, each with energy

$$E(q) = \left(\overline{n_q} + \frac{1}{2}\right)\hbar\omega(q) \tag{1.2}$$

where q represents the direction of wave propagation. For single crystals, one takes advantage of the symmetry, and represents the directional dependence of vibrational frequencies in the Brillouin zone. The relations $\hbar\omega(q)$ are known as dispersion relations which describe the effective forces acting on atoms in a given direction. We gain a more detailed understanding of thermal and elastic properties of crystals when phonon dispersion relations can be measured. Inelastic neutron scattering provides an established method for determining these relations [1]. Figure 1 shows phonon dispersion relations for α-Fe, measured by means of inelastic neutron scattering [2], and the phonon density of states derived from these relations using a formalism originally developed by Gilat and Raubenheimer [3]. Iron is chosen since it has a very suitable isotope with a long-lived Mössbauer transition, which is relevant to our discussion

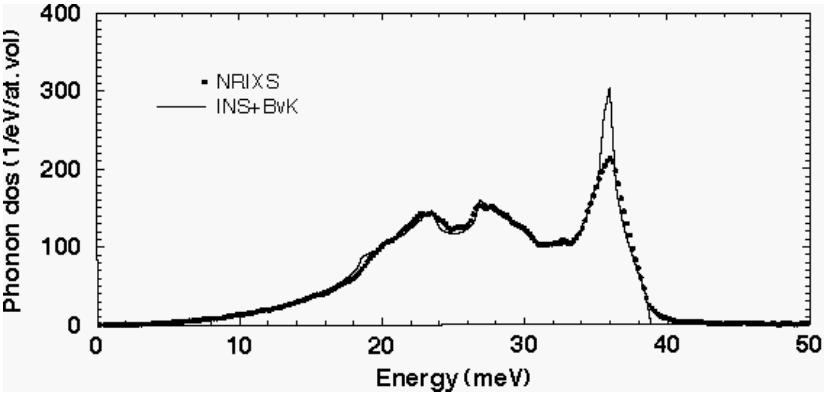

Figure 1. α-Fe phonon dispersion relations and the density of states for a-Fe. The phonon dispersion relations are measured by means of coherent inelastic neutron scattering (full curve) and the data are fitted to a set of force constants. The density of states obtained from sampling of the dispersion relations is compared to nuclear resonant inelastic x-ray scattering (NRIXS) data. The resolution of the NRIXS data was 0.8 meV.

in the following sections. The other isotopes used currently in the new technique that will be described here are isotopes of Kr, Eu, Sn, Sm, Dy, and this group could can be extended to include a number of others with some effort. The relevant properties of these isotopes are given in table 1.

Table 1. Relevant characteristics of Mössbauer isotopes suitable for INRXS experiments. The relative strength is the ratio of the normalized nuclear resonant scattering cross-section to that of iron. The normalization is with respect to nuclear and electronic cross-sections.

	E (keV)	Γ (neV)	$t_{1/2}$ (ns)	Relative strength
^{83}Kr	8.41	3.1	147.0	0.2
^{57}Fe	14.413	4.66	97.8	1.0
^{151}Eu	21.53	47	9.7	0.63
^{119}Sn	23.88	25.7	17.75	6.7
^{161}Dy	25.66	16.2	28.1	1.2

Before the experimental verification of the crystalline nature of solids by Bragg, Debye proposed a continuum model in 1911 that accounts well for low-temperature specific heat. Although this model only accounts for low-energy phonons whose wavelengths are longer than the interatomic distance, it is quite successful in explaining many properties of solids and liquids. If the wavelength of the vibrational excitation is much smaller than the interatomic distance, then the normal modes of vibration for the atom are the same as those for a crystal. For a crystal with N atoms, with $3N$ acoustic modes:

$$3N = \int_0^{\omega_D} \mathrm{d}\omega\, g(\omega) = \frac{V}{2\pi^2}\frac{\omega_D^3}{c_s^3} \tag{1.3}$$

where V is the volume of the unit cell, $g(\omega)$ is the density of vibrational modes between ω and $\mathrm{d}\omega$, and s refers to either one longitudinal or two transverse components of the acoustic mode, we have

$$\frac{3}{c_s^3} = \sum_s \frac{1}{c_s^3}. \tag{1.4}$$

The Debye cut-off frequency ω_D is introduced as a way of normalizing the number of modes to $3N$. This frequency helps define two quantities, the Debye temperature:

$$k\Theta_D = \hbar\omega_D \tag{1.5}$$

and the average sound velocity:

$$\omega_D = c_s\left(6\pi^2\frac{N}{V}\right)^{1/3}. \tag{1.6}$$

For real systems, the phonon density of states differs considerably from the Debye model, especially for large momentum-transfer values where the linear dispersion may disappear. This is a common feature of all periodic systems, as discovered by van Hove [4]. Thermodynamic properties of materials are expressed in terms of the real density of states as follows:

$$C_V = k\int_0^{\infty} \frac{\mathrm{e}^{\hbar\omega/kT}}{\mathrm{e}^{\hbar\omega/kT}-1}\left(\frac{\hbar\omega}{kT}\right)^2 g(\omega)\,\mathrm{d}\omega \tag{1.7}$$

$$C_P = C_V\left(1 - \frac{T}{\omega}\frac{\partial\omega}{\partial T}\right) \tag{1.8}$$

and

$$S = 3k\int_0^\infty g(\omega)\left[\frac{\hbar\omega}{2kT}\frac{e^{\hbar\omega/kT}+1}{e^{\hbar\omega/kT}-1} - \ln(e^{\hbar\omega/2kT} - e^{-\hbar\omega/2kT})\right]d\omega \tag{1.9}$$

where $\overline{\omega}$ is the average frequency.

As we see, the exact computation of C_V depends on the detailed knowledge of $g(\omega)$, which is here approximated by

$$g(\omega) = \frac{3V}{2\pi\hbar^3 c_s^3}E^2. \tag{1.10}$$

We will see an immediate application of (1.10) in section 5.

2. Observation of phonons by means of inelastic x-ray scattering

When electromagnetic radiation is scattered by lattice vibrations, the interaction is between the oscillating electric field vector of the photon and the oscillating electric charges. This interaction is subject to energy and momentum conservation:

$$E_i - E_f = \pm\hbar\omega \tag{2.1}$$

$$k - k' = Q. \tag{2.2}$$

The latter equation will be equally valid if a reciprocal-lattice vector G is added to the left side of equation (2.2) due to translational symmetry. In equation (2.1) the + sign refers to phonon creation, while the − sign refers to phonon annihilation.

In a typical scattering experiment, the goal is to find the change in energy as a function of change in angle (see figure 2). The energy of the electromagnetic radiation used for dynamical studies varies from the infrared to well into the γ-ray region. In the x-ray region, $5 < E < 30$ keV, there is a large mismatch between the incident beam energy of the photon and the absorbed energy. Thus, x-ray experiments require a resolution power of 10 keV/1 meV $\approx 10^7$ or better. This level of resolution can be accomplished with Bragg diffraction from high-order perfect crystals. Energy analysis of the scattered beam is accomplished by using spherically bent-crystal analysers working near backscattering [5–7]. This approach to measuring phonon dispersion curves requires samples to be single crystals with suitable dimensions. The size of the single crystal is limited not only by availability but also by the incident beam energy. For crystals with low atomic number, the size of the crystal must exceed several millimetres in order to contain sufficient electrons to scatter the x-rays. This may impose some inherent limitations in terms of studying materials under extreme conditions like high pressure and temperature. Another difficult sample geometry for this approach is that for the study of thin films or interfaces.

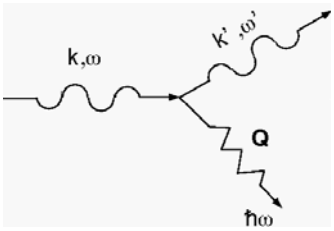

Figure 2. A typical x-ray scattering experiment involves a change in energy and momentum of the incident beam, yet obeying the conservation laws. Note that ω for the photons and ω for phonons are not the same, although the same notation is customarily used.

A different approach to the study of lattice excitations is to use a Mössbauer transition as an analyser, as the energy of the incident beam is scanned through the resonance energy. This is described in the next section.

3. Inelastic nuclear resonant x-ray scattering and the phonon density of states

The interaction between x-rays and atoms is quite complex because there are a number of different mechanisms taking place simultaneously. While the core electrons themselves can be displaced and ejected from the atom to a vacuum or continuum level, leading to a photoelectric cross-section, scattering from valence electrons which can be in extended orbitals as in metals leads to Compton scattering. The ejection of core electrons is followed by internal relaxation that leads to fluorescence radiation. For some atoms, it is also possible that x-rays in the range of 6–100 keV can interact with the nuclei, exciting internal energy levels with different angular momenta. The resulting excitations can be quite long lived. For example, after the release of an electron from a K shell, the ensuing atomic relaxation and restructuring involving the emission of K fluorescence may take place in 10^{-15} s. On the other hand, a nuclear excited state can last 10^{-7} s or even longer and creates its own delayed decay products of electrons and photons. A simplified schematic description is given in figure 3 for ^{57}Fe. In addition, nuclei with relatively low-lying excited states (i.e. below 100 keV) may undergo radiative transitions with no exchange of energy with the emitting or absorbing nuclei, the total momentum being transferred to the entire crystal. This recoilless emission or absorption of radiation is known as the Mössbauer effect, and it only occurs with a finite probability when the nuclei are bound in a solid. This probability, known as the recoil-free fraction or f-factor, is related to the mean square displacement by

$$f_{\mathrm{LM}} = \mathrm{e}^{-k^2\langle u^2\rangle} \tag{3.1}$$

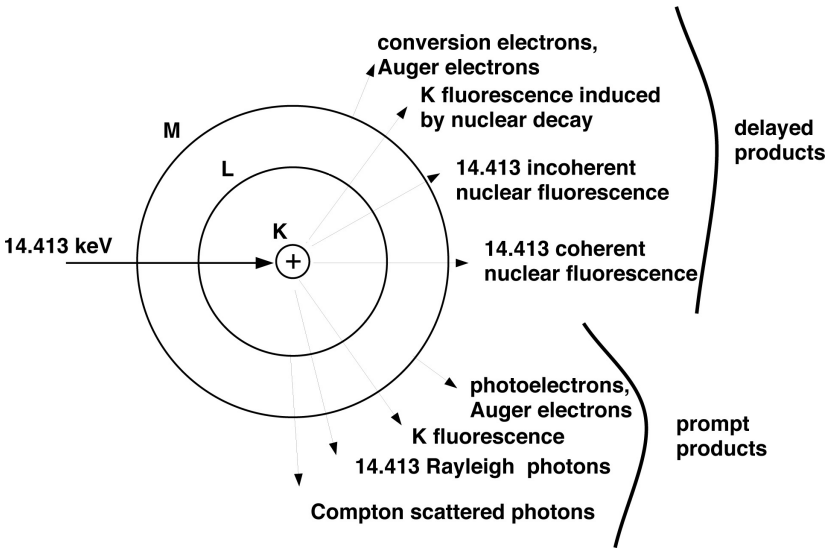

Figure 3. A simplified description of partial events during absorption and re-emission of 14.413 keV photons on ^{57}Fe-containing material. In a typical experiment, delayed K fluorescence of 6.4 and 7.05 keV (K_α and K_β) is detected as a function of incident photon energy.

where u is the displacement of atoms from their equilibrium position, and $k = 2\pi/\lambda$ is the total momentum of the x-ray photon emitted or absorbed. The subscript LM refers to Lamb and Mössbauer whose original articles on resonant capture of neutrons [8] and γ-rays [9] contributed to the basic understanding that we have today.

In a typical Mössbauer spectroscopy experiment, as shown in figure 4, the radioactive source moves against a sample with a frequency of about 25 Hz, in a constant-acceleration drive, with a velocity between ± 10 and 100 mm s^{-1}. The transmitted radiation depends on the relative Doppler shift that the radioactive source has experienced, and a spectrum is recorded as a function of velocity. The amount of Doppler shift is typically in the range of μeV, although this can be extended to meV, albeit with a low duty cycle [10]. Mössbauer spectroscopy is used to measure the strength and direction of hyperfine fields acting on the nuclei. In addition, it can be used to study lattice dynamics by measuring the recoil-free fraction of the resonance. This can be accomplished by measuring the change in the area of the Mössbauer resonance

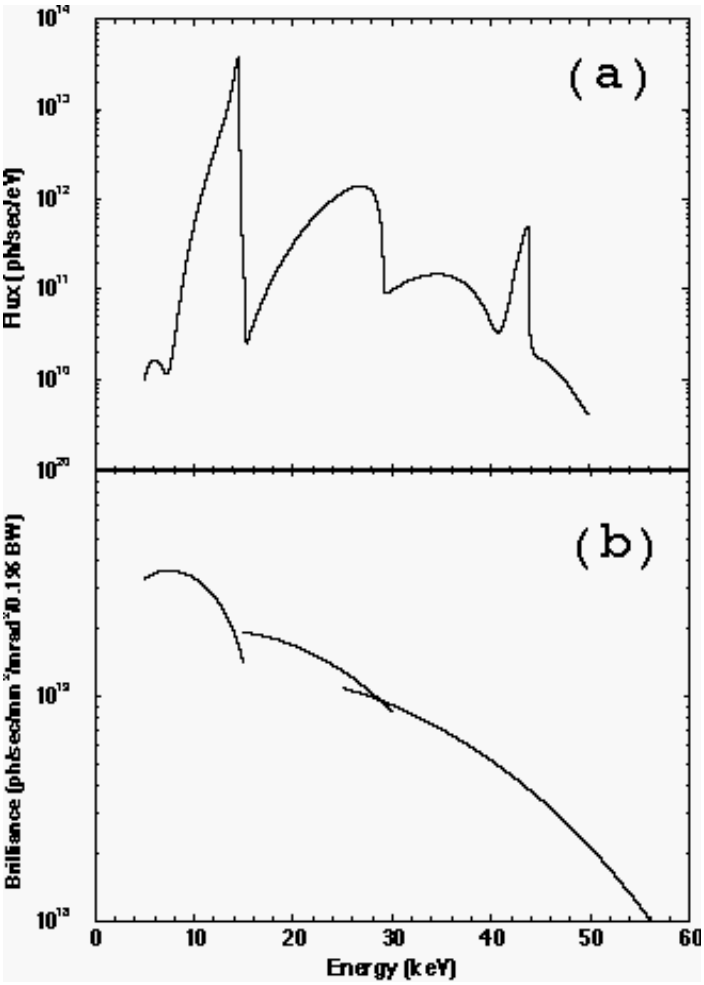

Figure 4. (a) The energy spectrum of the undulator at the 3-ID beamline of the Advanced Photon Source for a given gap and (b) the energy tunability range of the same undulator covered by the first few harmonics in the 5–50 keV range.

as a function of temperature. The Lamb–Mössbauer factor can then be calculated either by applying a technique known as 'transmission integration', or by comparing the temperature dependence of the area under the absorption peaks with the calculated curves for different Debye temperatures:

$$f_{\mathrm{LM}} = \exp(-R)\exp\left(\frac{3}{3k\Theta_D}\left[1 + \frac{4T^2}{\Theta_D^2}\int_0^{\Theta_D}\frac{x}{\mathrm{e}^x - 1}\,\mathrm{d}x\right]\right). \tag{3.2}$$

The second exponential term is graphically plotted for various values of Θ_D for over 30 isotopes in handbooks (e.g. [11]) and the f-factor can be obtained by comparison or numerical fitting. The first approach of transmission integration requires accurate knowledge of the thickness, concentration, and isotopic abundance, as these quantities enter into the formulation as a product [12]. The second approach may be limited if there is a phase transformation as a function of temperature. The method of inelastic nuclear resonant x-ray scattering, INRXS, on the other hand, yields the f-factor directly from a single measurement at a given temperature.

The radioactive source in the Mössbauer experiments can be replaced with a synchrotron source, which provides a number of benefits that change the nature of the experiments qualitatively. This is due the fact that synchrotron radiation emitted from undulators is intense (10^{13} photons s^{-1} eV^{-1}), well collimated (8–12 μrad vertically and 20–40 μrad horizontally), polarized, and pulsed. In terms of brightness (i.e. number of photons per unit time, per unit source area, and per unit angle), a synchrotron radiation source can be as much as a million times brighter than a sealed source of 100 Ci. The combination of all four qualities mentioned above enables new experiments that cannot be performed otherwise. Before we discuss the inelastic x-ray spectrum obtained by INRXS, we will look at some of the technical details involving the time and energy characteristics of the synchrotron radiation emitted from storage rings. The discrete nature of electron bunches in a storage ring provides a unique opportunity to excite a nuclear transition with or without phonon contributions, and detect it with the help of nucleus- or electron-induced fluorescence. For example, the storage ring at the APS has a circumference of 1108 m. When 24 radio-frequency buckets out of 1296 possible ones are filled with electrons, there will be 154 ns separation between the adjacent buckets. This number varies considerably for each facility, and different filling patterns allow bunch-to-bunch separation from a few nanoseconds to a few microseconds. The typical bunch length is about 50 ps.

Synchrotron radiations emitted from bending magnets and undulators have different characteristics in terms of energy spread and degree of collimation. Since the relevant x-ray source for state-of-the-art inelastic x-ray spectrometers is an undulator source, we will discuss its properties. An undulator is a device with a series of permanent magnets with alternating field directions perpendicular to the direction of the electron velocity and to the plane of the storage ring, causing electrons to oscillate sinusoidally with a period of a few centimetres. The spectrum emitted from the undulator source for the inelastic x-ray scattering beamline at the Advanced Photon Source is given in figure 4. The bandwidth of the first harmonic shown in the figure as a peak in the 14 keV region is around 600 eV (FWHM). The further reduction of the energy band-pass, first to a level of eV and then to meV (figure 5), is achieved by a set of crystal monochromators. A typical high-resolution monochromator can achieve a resolution power of 10^7 with an efficiency of about 50%. A detailed discussion of high-resolution monochromators is given in a recent review [13]. An important aspect of these monochromators is the energy tunability with a range orders of magnitude larger than that of a typical phonon spectrum. The discrete time structure of synchrotron radiation provides an unparalleled signal-to-noise ratio since the signal related to phonons comes at a time when

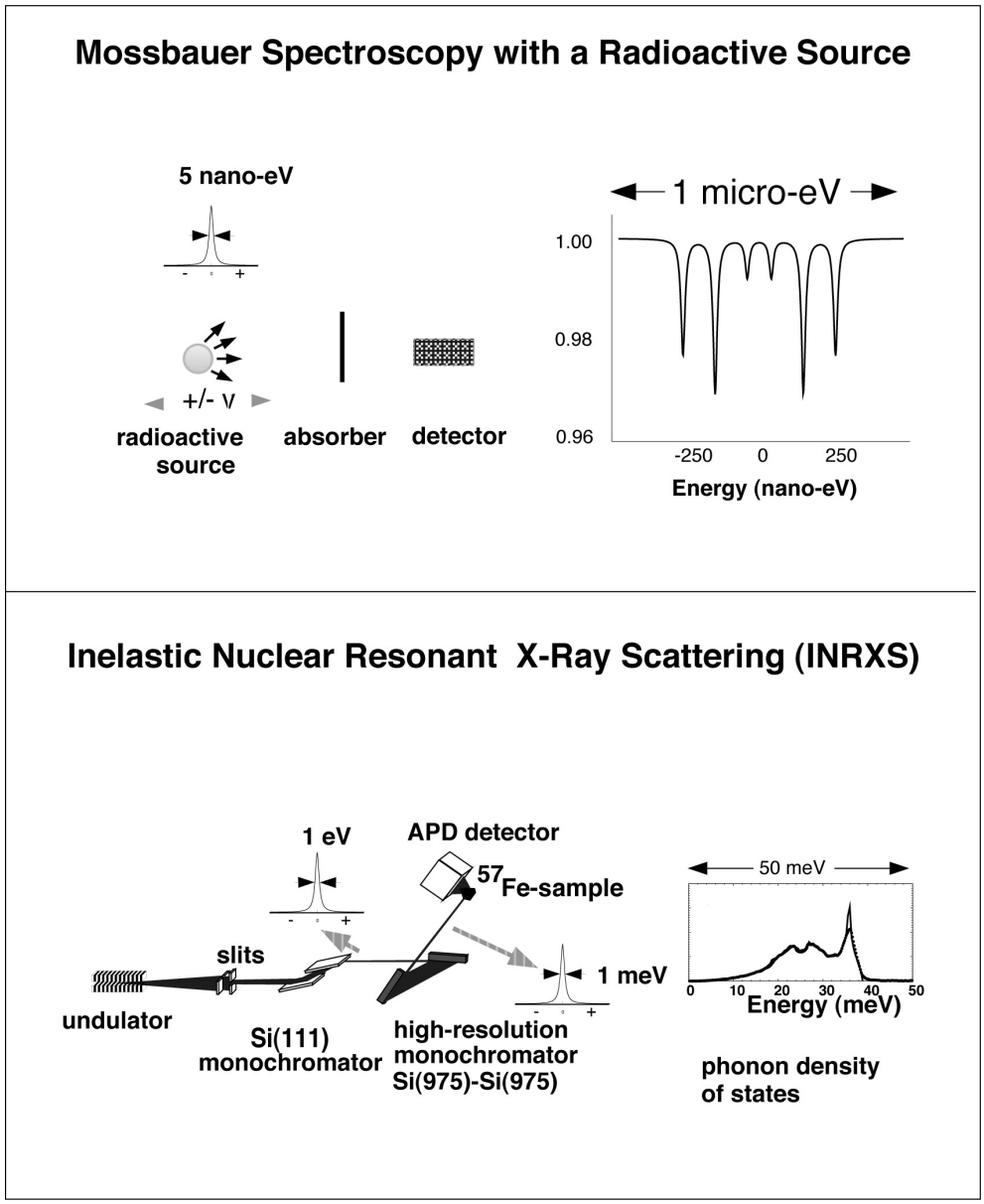

Figure 5. The schematic description of measuring excitation from a radioactive source and from a synchrotron source. In principle, the roles can be completely reversed, and one can get either hyperfine (i.e. neV level) excitation from the synchrotron set-up in a coherent forward-scattering experiment, or the phonon density of states from the radioactive source. However, the energy mismatch makes the last experiment very inefficient.

all other processes such as Compton scattering, Rayleigh scattering, and atomic fluorescence are bunched together and disappear within the detector resolution time. The state-of-the-art solid-state detectors with appropriate time resolution are avalanche photo-diodes (APD) with time resolutions of 0.1–1 ns, and a dynamic range of 10^8 [14].

Nuclear resonant scattering of synchrotron radiation and its applications have been recently reviewed [14], and it is not our intention to summarize these benefits here. We will limit ourselves to the extraction of thermal and elastic properties.

The INRXS experiments involve measurement of the intensity of delayed photons as a function of energy across a nuclear resonance:

$$I(E) = I_0 \rho \sigma(E). \tag{3.3}$$

Here, I_0 is the incident photon intensity, ρ is the density of nuclear resonant nuclei in the sample, and $\sigma(E)$ is the total interaction cross-section. The measured intensity is related to the absorption cross-section of nuclear resonance as well as the absorption probability associated with phonon exchange when the incident energy is far away from the resonance energy:

$$\sigma(\boldsymbol{k}, E) = \sigma_0 \frac{\alpha}{1+\alpha_T} \frac{\pi}{2} \Gamma \eta_f S(\boldsymbol{k}, E). \tag{3.4}$$

Here, σ_0 is the nuclear resonance cross-section given by

$$\sigma_0 = \frac{\lambda^2}{2\pi} \frac{2I_e + 1}{2I_g + 1} \frac{\Gamma_r}{\Gamma}. \tag{3.5}$$

Γ_r and Γ are partial linewidths, α and α_T are partial and total internal conversion coefficients related to the branching of nuclear decay products into electronic and nuclear fluorescence, and η_f is the electronic fluorescence yield followed by nuclear absorption and re-emission. For ^{57}Fe, the transition energy $E_0 = 14.4125$ keV, the linewidth Γ is 4.66 neV, and σ_0 is 2.56×10^{-18} cm^2. The $\boldsymbol{k}$-dependence of $\sigma(\boldsymbol{k}, E)$ can be dropped if the lattice is isotropic.

The measured intensity is actually a convolution of the interaction cross-section and the energy resolution function of the high-resolution monochromator, attenuated by the electronic absorption, both upon incidence and exit. A typical spectrum is given in figure 6(a). $S(\boldsymbol{k}, E)$ in equation (3.4) is the absorption probability due to phonons, and it is related to the self-correlation function $G_s(\vec{r}, t)$ [4] by a double Fourier transform in space and time:

$$S(\boldsymbol{k}, E) = \frac{1}{2\pi} \int \mathrm{d}t \, \mathrm{d}\vec{r} \, \mathrm{e}^{\mathrm{i}(\boldsymbol{k}\cdot\vec{r} - \omega t)} G_s(\vec{r}, t). \tag{3.6}$$

The phonon absorption probability has an elastic and an inelastic component, which can be separated:

$$S(E) = f_{\mathrm{LM}} \delta(E) + S'(E) \tag{3.7}$$

where f_{LM} is the recoil-free fraction, or Lamb–Mössbauer factor mentioned earlier in relation to equation (3.1), and $S'(E)$ is the inelastic part which is of main interest here. The inelastic part of the spectrum is composed of contributions from single-phonon and multiphonon scattering:

$$S'(E) = S'_1(E) + S'_2(E) + S'_3(E) + \cdots. \tag{3.8}$$

The procedural details for extracting the single-phonon density of states, $D(E)$, are given elsewhere in detail [16–20]. Figure 6(b) shows the relative sizes of the one-, two-, and three-phonon contributions to the iron spectrum at room temperature. The explicit relationship between the single-phonon absorption cross-section and the phonon density of states is given by

$$D(E) = \frac{3E}{E_R} \frac{S'_1(E)}{f} \left[1 - \mathrm{e}^{-E/kT}\right]. \tag{3.9}$$

This result relates an experimentally measured quantity, $S(E)$, to a fundamental property of the sample, the phonon density of states, $D(E)$. As we saw in equations (1.7)–(1.9), specific heat and vibrational entropy are directly related to $D(E)$, as is the speed of sound, as given in equation (1.10).

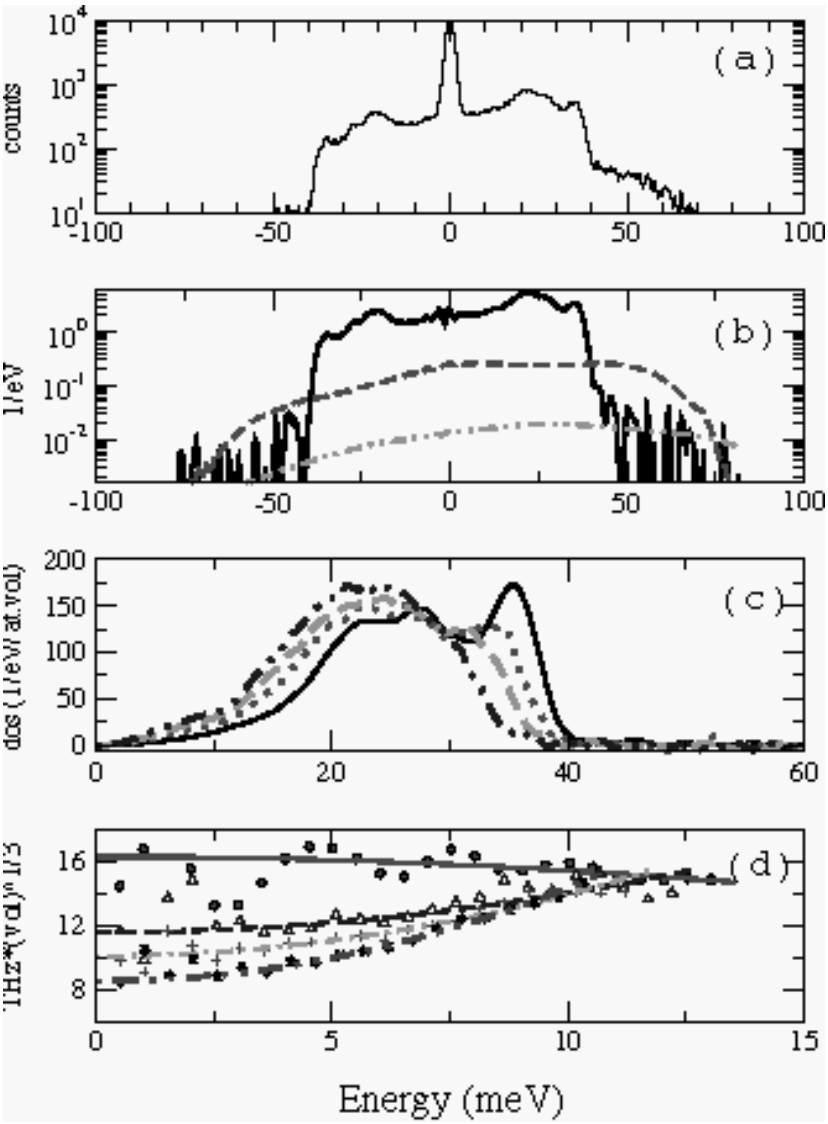

Figure 6. (a) The measured nuclear resonant inelastic x-ray scattering (NRIXS) signal. (b) The decomposition of the total absorption probability into (full curve) one-phonon, (broken curve) two-phonon, and (chain curve) three-phonon components. (c) The phonon density of states from (full curve) bulk α-Fe, (dotted curve) Fe(20 Å)/Au(20 Å), (dashed curve) Fe(10 Å)/Au(10 Å), and (chain curve) Fe(5 Å)/Au(5 Å) multilayers. (d) Sound velocity for (●) bulk α-Fe, (Δ) Fe(20 Å)/Au(20 Å), (+) Fe(10 Å)/Au(10 Å), and ($*$) (Fe(5)/Au(5 Å) multilayers.

Study of lattice excitations by means of scattering x-rays was among the first applications of x-rays to crystals. X-rays with energy $\hbar\omega$ and momentum k can be scattered from atoms and nuclei, carrying information about the energy and momentum distribution. In fact, an analysis of the energy spectrum and its moments is the crucial part of all x-ray scattering experiments, since it reflects the vibrational characteristics of the scattering centres with high fidelity. The scattering process can be considered as radiation emitted from an induced dipole. The atomic

or nuclear charge, excited by the incident radiation, was occupying an initial state $|i\rangle$, and after the interaction with the radiation, it is transferred to a final state $|f\rangle$. The energy of the photon E_γ is shifted from initial energy E_0 by the energy lost due to recoil, R:

$$E_\gamma = E_0 - R \tag{3.10}$$

assuming that the nucleus was isolated, and initially at rest. For a moving nucleus with mass M and velocity v_i,

$$E_\gamma = E_0 - R + \frac{\hbar^2 k' k}{2M} \tag{3.11}$$

where $\hbar k'/(2M)$ is the initial momentum of the atom. The atoms in solids are bound in a lattice (irrespective of periodicity), and they have a distribution of velocities. However, this distribution is not continuous like the Maxwellian distribution in ideal gases, but rather is discrete due to the quantized nature of the atomic vibrations. In fact, it is customary to represent the motion of atoms within the formalism of a harmonic oscillator, with quantized energy levels $(n + \frac{1}{2})\hbar\omega$, where ω here relates to the oscillation frequency of atoms, $\omega/(2\pi)$. The spacing between the energy levels n is proportional to the stiffness of the lattice. When we deal with a large number of oscillators, the expectation values of various moments of the energy distribution can be calculated. According to Lipkin [21],

$$\langle E_\gamma^m \rangle = \langle i | \left(E_0 - H + E_{n'} + \frac{\hbar k p}{M} - R \right)^m | i \rangle \tag{3.12}$$

where

$$H = \frac{p^2}{2M} + \frac{1}{2} m\omega^2 x^2$$

is the Hamiltonian for a harmonic oscillator with mass M and oscillation frequency $\omega/(2\pi)$. The most intriguing aspect of (3.12) is that it relates the moments of the distribution of the measured x-ray spectrum to those of the energy states of the system.

The first three moments of the energy spectrum have been calculated [21, 22]:

$$\begin{aligned} \langle E_\gamma^1 \rangle &= R \\ \langle E_\gamma^2 \rangle &= 4R\overline{T} \\ \langle E_\gamma^3 \rangle &= R\hbar^2 \overline{\omega_z^2} = \left(\frac{2\hbar^2 R}{M} \right) \frac{\partial^2 U_\mu}{\partial z^2}. \end{aligned} \tag{3.13}$$

R, the recoil energy, is given by $E_\gamma^2/(2Mc^2)$,

$$\overline{T} = \frac{\langle i | p_{z\mu}^2 | i \rangle}{2M}$$

is the mean kinetic energy along the beam direction z for the atom μ, and $\overline{\omega_z^2}$ is the weighted mean square average of the frequency which is related to the force constant along the z-direction. The discussion here is quite general, and it applies to resonant as well as non-resonant scattering.

4. Thermal and elastic properties extracted from the phonon density of states

We can now take a look at the thermal and elastic quantities that can be extracted from measurement of NRIXS spectra. These quantities are the f-factor, the second-order Doppler shift, the internal kinetic energy, the specific heat, the vibrational entropy, the force constant, and the sound velocity.

The recoil-free fraction mentioned in the previous section can be calculated directly from the phonon DOS as follows:

$$f_{\mathrm{LM}} = \exp\left(-R\int_0^{\omega_D} \frac{g(\omega)}{\omega}\frac{1+\mathrm{e}^{-\hbar\omega/kT}}{1-\mathrm{e}^{-\hbar\omega/kT}}\,\mathrm{d}\omega\right) = \mathrm{e}^{-k^2\langle u^2\rangle}. \tag{4.1}$$

The recoil-free fraction is a quantity closely related to the Debye–Waller factor, a constant that can be measured from the reduction of the x-ray diffraction intensity. The two quantities are related to each other by

$$f_{\mathrm{DW}} = \mathrm{e}^{-q^2\langle u^2\rangle}. \tag{4.2}$$

The difference between the quantities comes from the momentum transfer. In a forward-scattering experiment, all of the momentum, k, is transferred, while in a diffraction experiment, this is modified by the scattering angle, $q = 4\pi(\sin\theta)/\lambda$.

Equation (3.13), which involved no assumption as regards a particular model, relates the second and third moments of the inelastic x-ray spectrum to the kinetic energy and average force constant, and it is directly obtained from the moments of the spectrum.

We finish this section with an application to a multilayer system. The phonon density of states of thin films coated on a substrate was first measured by carefully adjusting the critical angle of incidence of the substrate and the coated film to increase the yield of the delayed nuclear fluorescence radiation [23]. In this geometry, the photon beam is incident upon a flat coated substrate at a grazing incidence angle steep enough for it to penetrate the film, but shallow enough for it to be reflected by the substrate which has a larger electron density. A typical incidence angle of a few milliradians creates a footprint a few centimetres long. This would represent a rather extended source if it were to be analysed by another set of crystal optics. However, in INRXS experiments the analyser is built into the sample in the form of resonant nuclei. Therefore, a detector with a large surface area placed a few millimetres away from the surface is adequate. The INRXS method has been applied to study the effect of film thickness [23] and film composition [24] on the phonon density of states. Furthermore, multilayers and buried interfaces are studied with this method. The films were prepared by sputtering to demonstrate the feasibility of INRXS experiments using small quantities of materials.

As examples, the phonon densities of states of Fe/Au multilayers as functions of the thicknesses of the Fe and Au layers are given in figure 6(c). As the layer thickness is decreased, the high-energy modes of Fe around 35 meV are suppressed, and some new energy states at low energy appear. The recoil-free fraction and kinetic energy and specific heat that are extracted from the data are given in table 2. There is a softening of the lattice in the Fe layers with decreasing thickness, as evidenced by the reduction of the f-factor as well as the force constant. The speed of sound, which is related to the density of states as given in equation (1.10), can be extracted form the low-energy part of the density of states, as shown in figure 6(d). The reduction of the speed of sound is consistent with the reduction in the force constant and recoil-free fraction.

Table 2. Derived thermal and elastic properties of Fe and Fe/Au multilayers.

Material	f-factor	Kinetic energy (meV/atom)	C_V (k_B/atom)	c_s (THz (vol)$^{1/3}$)	Force constant (N m^{-1})
α-Fe	0.794	14.2	2.7	15.46	168
Fe(20 Å)/Au(20 Å)	0.73	13.9	2.76	12.63	151.5
Fe(10 Å)/Au(10 Å)	0.68	13.8	2.79	11.3	130
Fe(5 Å)/Au(5 Å)	0.64	13.7	2.81	10.3	117

A second example relating to thin films is given in figure 7. A set of Fe/Cr multilayer films were prepared in each of which a monolayer of ^{57}Fe is deposited either at the interface or in the interior of the Fe layers, and the phonon densities of states of these layers are compared to that of bulk iron, as well as that of ^{57}Fe as an impurity in Cr metal. The four phonon densities of states shown in figure 7 are indicative of the power of this new method in terms of combining thin-film applications with elemental—and better still with isotope—selectivity. The details of the film preparation are given elsewhere [24].

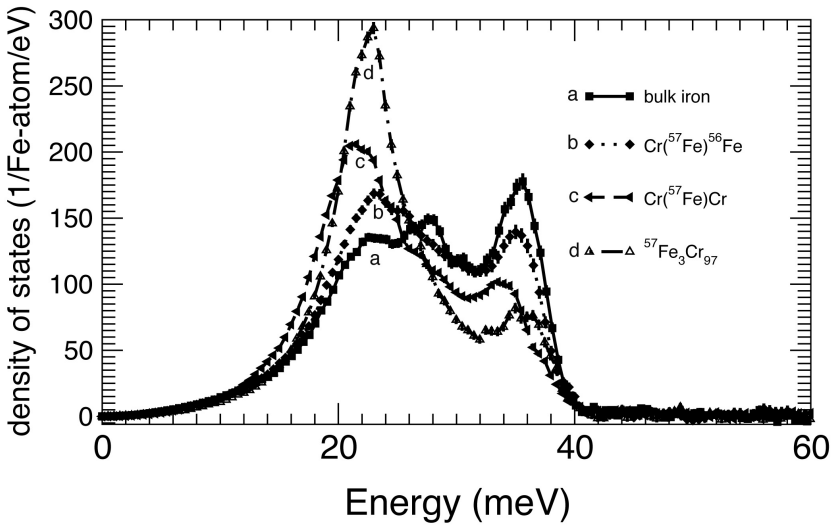

Figure 7. Element and isotope selectivity is combined to demonstrate the effect of near neighbours on the density of states of ^{57}Fe in Fe/Cr multilayers [24]. The bulk iron phonon DOS (a) is compared with that of ^{57}Fe at the iron–chromium interface (b), that of ^{57}Fe inside the ^{56}Fe layer in the Fe–Cr multilayer (c), and that of 3% ^{57}Fe distributed as point defect inside pure chromium (d). The thicknesses of the Fe/Cr layers were about 11.5 Å, and the 200 layers were deposited onto a 1 cm^2 area. The energy resolution for these measurements was 2 meV.

5. Perspectives

The method of INRXS presented here is still in its infancy as a fundamental physical measurement technique. The recent applications to materials under high pressure [25] and the study of the long-range dynamics of protein molecules [26] indicate that unique applications will continue to appear in the next few years. Also, the minimum achievable energy resolution is continuously being improved on—currently it is a few hundred μeV [27, 28]—and there is a real possibility that it can be reduced even further. This, coupled with improvements in APD detectors, makes the INRXS technique appear likely to be increasingly useful over the next decade.

Acknowledgments

We would like to thank our collaborators who worked at the SRI-CAT 3-ID beamline at the APS, in particular Drs M Hu, J Zhao, R Röhlsberger, H Sinn, W Keune, G Bortel, K Quast, and P Lee, for their contributions over many years, during which time the INRXS method was

being developed. This work was supported by the US Department of Energy under contract No W-31-109-ENG-38.

References

[1] Marshal W and Lovesey S W 1971 *Theory of Thermal Neutron Scattering* (London: Oxford University Press)
[2] Minkiewicz V J, Shirane G and Nathans R 1967 *Phys. Rev.* **162** 528
Landolt–Börnstein New Series 1981 Group III, vol 13, ed K-H Hellwege and J L Olsen (Berlin: Springer) pp 53–6
[3] Gilat G and Raubenheimer L J 1965 *Phys. Rev.* **144** 390
[4] van Hove L 1954 *Phys. Rev.* **95** 249
[5] Dorner B, Burkel E, Illini Th and Peisl J 1987 *Z. Phys.* B **69** 179
[6] Burkel E, Peisl J and Dorner B 1987 *Europhys. Lett.* **3** 957
[7] For a recent review of inelastic x-ray spectrometers, see Sinn H *et al* 2001 *J. Phys.: Condens. Matter* **13**
[8] Lamb W E Jr 1938 *Phys. Rev.* B **55** 190
[9] Mössbauer R L 1958 *Z. Phys.* **151** 124
[10] Weiss H and Langhoff H 1979 *Phys. Lett.* A **69** 448
Weiss H and Langhoff H 1979 *Z. Phys.* B **33** 365
[11] Callis G H M and Baker R J 1981 *Handbook of Spectroscopy* vol 3, ed J W Robinson (Boca Raton, FL: Chemical Rubber Company Press) p 424
[12] Margulies S and Ehrman J R 1961 *Nucl. Instrum. Methods* **12** 131
[13] Toellner T S 2000 *Hyperfine Interact.* **125** 3
[14] Kishimoto S 1992 *Rev. Sci. Instrum.* **63** 824
[15] Gerdau E and DeWaard H (ed) 1999–2000 *Nuclear Resonant Scattering of Synchrotron Radiation; Hyperfine Interact.* **123–125**
[16] Sturhahn W *et al* 1995 *Phys. Rev. Lett.* **74** 3832
[17] Chumakov A and Sturhahn W 1999 *Hyperfine Interact.* **124** 781
[18] Chumakov A 1999 *Hyperfine Interact.* **124** 809
[19] Sturhahn W 2000 *Hyperfine Interact.* **125** 149
[20] Hu M *et al* 1999 *Nucl. Instrum. Methods* A **428** 551
[21] Lipkin H 1960 *Ann. Phys., NY* **9** 332
Lipkin H 1973, 1986 *Quantum Mechanics* (Amsterdam: North-Holland)
[22] Lipkin H 1995 *Phys. Rev.* B **52** 10 073
[23] Röhlsberger R *et al* 1999 *J. Appl. Phys.* **86** 584
[24] Keune W and Sturhahn W 1999 *Hyperfine Interact.* **123+124** 847
[25] Mao H K *et al* 2001 *Science* **292** 914
[26] Sage J T *et al* 2001 *Phys. Rev. Lett.* **86** 4966
[27] Toellner T 2001 *J. Synchrotron Radiat.* **8** 1082
[28] Baron A *et al* 2001 *J. Synchrotron Radiat.* at press